npj | computational materials

Article

Published in partnership with the Shanghai Institute of Ceramics of the Chinese Academy of Sciences

https://doi.org/10.1038/s41524-024-01438-9

Quantum-inspired genetic algorithm for designing planar multilayer photonic structure

Zhihao Xu [1], Wenjie Shang[1], Seongmin Kim [2], Alexandria Bobbitt[1], Eungkyu Lee [3] ✉ & Tengfei Luo [1,4] ✉

Quantum algorithms are emerging tools in the design of functional materials due to their powerful solution space search capability. How to balance the high price of quantum computing resources and the growing computing needs has become an urgent problem to be solved. We propose a novel optimization strategy based on an active learning scheme that combines the Quantum-inspired Genetic Algorithm (QGA) with machine learning surrogate model regression. Using Random Forests as the surrogate model circumvents the time-consuming physical modeling or experiments, thereby improving the optimization efficiency. QGA, a genetic algorithm embedded with quantum mechanics, combines the advantages of quantum computing and genetic algorithms, enabling faster and more robust convergence to the optimum. Using the design of planar multilayer photonic structures for transparent radiative cooling as a testbed, we show superiority of our algorithm over the classical genetic algorithm (CGA). Additionally, we show the precision advantage of the Random Forest (RF) model as a flexible surrogate model, which relaxes the constraints on the type of surrogate model that can be used in other quantum computing optimization algorithms (e.g., quantum annealing needs Ising model as a surrogate).

In the pursuit of continuous technological advancement in the field of materials science, the design and discovery of novel functional materials are always at the forefront of innovation. In practice, the performance of different functional materials is dependent on many design factors, such as geometrical features, composition, processing conditions, and environmental factors, which lead to large design spaces[1–3]. Traditional methods, including experiments and simulations, are usually too time-consuming and expensive to comprehensively search the extremely large design spaces. Therefore, for general functional material design problems (such as alloy materials, optical materials, etc.), although comprehensive physical models have been established, traditional design methods can still only explore a small part of the design space around the configurations that have been well investigated.

With the development of computational science and data science, machine learning algorithms begin to transform the field of material design. Taking the design of optical structures as an example, a series of deep learning-based algorithms combining forward modeling and inverse design have been proposed and applied in practice[4–6], by which an artificial neural network model would be trained as a surrogate to mimic computationally expensive physical simulations for evaluating the topology-property relationship. Then, a generative model, such as Generative Adversarial Networks (GANs)[5,7,8] or Variational Autoencoders (VAEs)[9–11], is used to inversely retrieve the design based on material properties[12–14].

Another widely used approach is to use machine learning models as surrogate models and combine them with global optimization algorithms. These surrogate model-based algorithms can effectively address the one-to-many challenge in many inverse design problems, i.e., there are multiple non-unique solutions to the same design target[12]. Compared to direct neural network inverse design, this approach heavily relies on the performance of the global optimization algorithm to iteratively search the optimization space. Some classical optimization algorithms such as Genetic Algorithm (GA, or classical GA) and Simulated Annealing algorithm (SA) have been widely applied for material design and optimization[15–19]. These algorithms can effectively explore the design space with limited information[20]. With the emergence and development of quantum computing, a variety of sophisticated, high-performance quantum algorithms have been employed to

[1]Department of Aerospace and Mechanical Engineering, University of Notre Dame, Notre Dame, IN, 46556, USA. [2]National Center for Computational Sciences, Oak Ridge National Laboratory, Oak Ridge, TN, 37830, USA. [3]Department of Electronic Engineering, Kyung Hee University, Yongin-si, Gyeonggi-do, 17104, Republic of Korea. [4]Department of Chemical and Biomolecular Engineering, University of Notre Dame, Notre Dame, IN, 46556, USA. ✉e-mail: eleest@khu.ac.kr; tluo@nd.edu

tackle complex and large-scale optimization problems, facilitating the material designing with surrogate-based algorithms. One example is the Quantum Annealing (QA) algorithm, which provides highly accurate solutions for a specific kind of combinatorial optimization known as Quadratically Constrained Binary Optimization (QUBO)[21–23]. However, for any problems that have complex optimization landscapes, utilizing QUBO as the surrogate model and solving it with QA has been the necessary strategy since QA can only work with QUBO-like models (e.g., the Ising model). The errors introduced by ignoring higher-order terms beyond the second order in the surrogate model require many iterations between QUBO training/retraining, QA, and data collection before convergence is achieved[24].

Motivated by quantum computing theories, some heuristic algorithms were proposed as the enhanced solution for classical algorithms. One of the representative examples is the Quantum-inspired GA (QGA). The QGA was first introduced by Narayanan et al. [25]. It is distinguished by its smaller population size, rapid convergence speed, robust global optimization capabilities, and strong resilience to variations in problem specifications[26,27]. QGA integrates the principles of quantum computing with the robustness of classical genetic algorithms, thereby enhancing the exploration capabilities and convergence speed. This approach leverages the superposition and entanglement of quantum information (i.e., vectors in Hibbert space), enabling the algorithm to explore multiple solutions simultaneously and avoid local optima more effectively. By combining these quantum principles with the adaptive search capabilities of genetic algorithms, QGA can provide a more efficient and scalable solution for complex optimization problems. The iterative process of QGA, which includes quantum-inspired mutation and crossover operations, maximizes a comprehensive search of the solution space, leading to higher precision and faster convergence compared to traditional methods[28].

The Planar multilayer (PML) system is very widely used in optoelectronics, photonic crystals, and anti-reflective coatings due to their simplicity in manufacturing and flexibility in design[29]. Recently, it has been used for the design of transparent radiative coolers (TRC)[30–32], which block non-visible solar light and prevent excessive heating of rooms or compartments[33–36] without external energy[29,37–39]. In general, PML structures consist of dielectric materials, metals or organic thin films with distinctive refractive indices, and a spectral response across the solar wavelength range can be determined by the special combination and order of the material layers in the PML structure. The optimization for PML can be formulated into a combinatorial optimization problem for the stack of different candidate materials[40]. As the number of material layers increases, the dimension of the optimization problem will rise to a level that is prohibitive for many traditional methods, and there will be lots of local optima present in the objective function. Researchers have proposed a variety of optimization strategies for exploring potential optimal PML structures, such as needle optimization[29,40,41], memetic method[42,43] and deep reinforcement learning[44]. However, these methods often encounter challenges with converging to local minima. Therefore, an advanced algorithm with exceptional good global search capabilities is needed. Kitai et al. [45] and Kim et al. [24] utilized quantum annealing (QA) and factorization machine (FM) for the design of PML. These algorithms, based on quantum annealing, deliver a superior optimization speed and precision compared to classical computers.

In this work, we introduce an optimization algorithm based on a QGA for binary combinatorial optimization problems. As a test case, we use it to design PML for TRC applications. This optimization algorithm can utilize general surrogate models and find the optimum by QGA. We choose the Random Forest (RF) as the surrogate model in this study. Numerical experiments are conducted for structures with 6 to 20 layers, and the results show that our QGA-facilitated optimization algorithm can converge to comparable solutions as QA and overperforms classical genetic algorithm (CGA) on both convergence speed and global search capability. Furthermore, due to the advantages brought by the RF model, fewer iterations are needed for the QGA to converge to the optimal solution compared with QA-facilitated optimization. The proposed method provides a powerful tool for solving binary combinatorial optimization problems with complex searching spaces.

Results

The Quantum Genetic Algorithm

In QGA, a quantum chromosome, composed of multiple qubits, represents a potential solution. This algorithm mimics the evolution of physical qubits undergoing quantum logic gates, where "qubits" and "quantum gates" refer to mathematical-quantum information and operators within the complex Hilbert space, respectively. The algorithm manipulates these chromosomes using quantum gates, analogous to genetic operations of crossover and mutation. Leveraging superposition, a quantum chromosome can represent multiple solutions simultaneously, vastly increasing the algorithm's ability to explore a large search space. The use of quantum entanglement can introduce correlations between qubits, enabling the algorithm to maintain a higher diversity of solutions and avoid premature convergence on local optima. These characteristics make QGA particularly suitable for complex optimization problems where traditional genetic algorithms may struggle due to the sheer size of the search space or the need for rapid convergence[46]. In addition, the evolution of quantum chromosomes can save memories by avoiding maintaining groups of binary vectors in CGA, which represent the population in the generation. QGA also utilizes the concept of quantum entanglement, enabling a more effective exchange of information between solutions. This makes QGA more adept at avoiding premature convergence to local optima, which is a common pitfall in CGA. In the evolution of QGA, the quality of the quantum chromosome is evaluated by calculating the fitness values of independent measurements of the quantum chromosome (the details of quantum measurement are in the Method section). The fitness values are evaluated by a figure-of-merit (FOM), which is used to describe how close between a designed PML structure and the ideal TRC. The FOM can be calculated by:

$$FOM = \frac{10\int_{\lambda_1}^{\lambda_2}\left(Tl(\lambda) - Tl_{ideal}(\lambda)\right)^2 d\lambda}{\int_{\lambda_1}^{\lambda_2} S(\lambda)^2 d\lambda} \tag{1}$$

(the details of the FOM and parameters definition are in the Supplementary Information, Section 1). Minimizing the FOM will allow the designed TRC to approach the ideal TRC, so that the fitness value in the QGA is defined as $f = -100 \times$ FOM. The measurements with high fitness values provide genetic information for the evolution direction of quantum chromosomes.

Compared with the CGA, QGA employs the probability amplitudes of qubits to encode chromosomes (as depicted in Eq. 12) and utilizes quantum rotation gates to execute the chromosomal updated operations. Consequently, the formulation of the quantum rotation gates serves as a critical aspect of QGA, directly influencing the algorithm's performance. Here, we apply rotation-Y (Ry) gates on each qubit in the chromosome to realize the evolution. The Ry gate can be defined in a matrix form as[28,47,48]:

$$Ry(\theta) = \begin{bmatrix} \cos\frac{\theta}{2} & -\sin\frac{\theta}{2} \\ \sin\frac{\theta}{2} & \cos\frac{\theta}{2} \end{bmatrix} \tag{2}$$

The updated process is:

$$\begin{bmatrix} a_k^{t+1} \\ b_k^{t+1} \end{bmatrix} = Ry\left(\theta_k^t\right)\begin{bmatrix} a_k^t \\ b_k^t \end{bmatrix} = \begin{bmatrix} \cos\frac{\theta_k^t}{2} & -\sin\frac{\theta_k^t}{2} \\ \sin\frac{\theta_k^t}{2} & \cos\frac{\theta_k^t}{2} \end{bmatrix}\begin{bmatrix} a_k^t \\ b_k^t \end{bmatrix} \tag{3}$$

where $[\alpha_k^{t+1}, b_k^{t+1}]^{\mathrm{T}}$ and $[\alpha_k^t, b_k^t]^{\mathrm{T}}$ represent the probability amplitudes of the k-th qubit in the chromosome at the $t+1$-th generation and the t-th generation, respectively. θ_k^t is the rotating angle for the Ry gate. We used an

Table 1 | Adjustment Strategy of Rotating Angle

x_i*	best$_i$	$f(x) > f(\text{best})$ **	θ	$s(a_i, b_i)$ ***			
				$a_i b_i > 0$	$a_i b_i < 0$	$a_i = 0$	$b_i = 0$
0	0	False	0	0	0	0	0
0	0	True	0	0	0	0	0
0	1	False	θ_i	+1	−1	0	±1
0	1	True	θ_i	−1	+1	±1	0
1	0	False	θ_i	−1	+1	±1	0
1	0	True	θ_i	+1	−1	0	±1
1	1	False	0	0	0	0	0
1	1	True	0	0	0	0	0

* x_i and best$_i$ represent the i-th bit of chromosomes and best individual, respectively.
** $f(\cdot)$ is the fitness evaluation function. The best individual has the highest fitness.
*** $s(a_i, b_i)$ is the direction of the rotating operation. +1 represents clockwise rotation.

adaptive adjustment strategy[28] for the quantum rotation angle so that the direction and magnitude are updated dynamically during the evolutionary process. A large rotating angle is set early in the evolutionary process to quickly explore the solution space and find regions likely to contain optimal values. To accurately find the optimal value, we reduce the magnitude of rotating angle as evolution continues so that it eventually converges to a global optimum. The update of rotating angle follows the following formula:

$$\theta_i = \theta_{\max} - \left(\frac{\theta_{\max} - \theta_{\min}}{N}\right) \times i \tag{4}$$

where θ_i is the value of the rotating angle of the i-th generation, N is the max generation, $\theta_{\max}$ and $\theta_{\min}$ is the upper bound and lower bound of θ. The adjustment strategy of rotating angle is shown in Table 1[49].

In the CGA, the crossover operation in the evolution allows for an expansive exploration of the solution space. However, the quantum chromosome itself has the property of individual diversity resulting from quantum superposition. So, there is no need to perform the crossover operation in the QGA. On the other hand, mutation is the operation that can ensure sufficient variety in the population to avoid local optima, which is important for both CGA and QGA. Different from CGA, quantum mutation will appear on the quantum chromosome and completely reverse the individual's evolutionary direction by swapping the value of probability amplitudes a and b of mutated qubits, which is implemented by X-Gate on the randomly selected qubits as[47]:

$$X = \begin{bmatrix} 0 & 1 \\ 1 & 0 \end{bmatrix}, X\begin{bmatrix} a_k^t \\ b_k^t \end{bmatrix} = \begin{bmatrix} b_k^t \\ a_k^t \end{bmatrix} \tag{5}$$

Additionally, at the start of each QGA iteration, the genetic information of the optimal individual obtained from the previous QGA iteration will be partially incorporated into the initialization of the quantum chromosome, which reinforces the retention and utilization of valuable genetic information, leading to more efficient convergence towards optimal solutions. Therefore, the initialization of the quantum chromosome q in iteration τ is:

$$\begin{aligned} q(\tau = 0) &= \left[Ry\left(\theta_k^{rand}\right) \cdot \begin{bmatrix} \frac{1}{\sqrt{2}} \\ \frac{1}{\sqrt{2}} \end{bmatrix}_k \text{ for } k = 1, 2, \ldots, n \right] \\ q(\tau > 0) &= \left[w_p \cdot \begin{bmatrix} a_k \\ b_k \end{bmatrix}^{it-1} + (1 - w_p) \cdot Ry\left(\theta_k^{rand}\right) \cdot \begin{bmatrix} \frac{1}{\sqrt{2}} \\ \frac{1}{\sqrt{2}} \end{bmatrix}_k \text{ for } k = 1, 2, \ldots, n \right] \end{aligned} \tag{6}$$

where θ^{rand} is the randomly generated initial angle between 0 to π, w_p is the weighing factor to balance the genetic information from prior QGA iteration and random initialization in the current iteration. Each qubit is firstly initialized to a uniform superposed state by the Hadamard gate as:

$$H = \frac{1}{\sqrt{2}}\begin{bmatrix} 1 & 1 \\ 1 & -1 \end{bmatrix}, H\begin{bmatrix} 1 \\ 0 \end{bmatrix} = \begin{bmatrix} \frac{1}{\sqrt{2}} \\ \frac{1}{\sqrt{2}} \end{bmatrix} \tag{7}$$

Then, a series of Ry gates with randomly generated angles is applied to each qubit to produce a random quantum chromosome for QGA. Except for the first QGA iteration, other iterations will start with the initialized quantum chromosome which also incorporates the solution of former QGA iteration with weighing factor w_p as shown in Eq. 6. The determination of w_p is based on the following formula:

$$w_p = \frac{1}{2}\frac{best_{current}}{best_{all}} \tag{8}$$

where $best_{all}$ and $best_{current}$ are the best fitness values of all time and in the current iteration, respectively. If the current iteration successfully converges to or exceed the fitness value of all time, $best_{all}$ will equal to $best_{current}$ at the end of the iteration, so that $w_p = 0.5$. Otherwise, $best_{all}$ will be higher than $best_{current}$ at the end of the iteration, which means that the initialization of the next iteration will have higher degree of randomness to encourage exploration of the entire landscape.

Additionally, to further mitigate the risk of the algorithm falling into a local optimum, we introduce an operation which we call memory corruption. This operation allows the optimal result, inherited from the previous cycle, to be discarded with a certain probability. This ensures that the incoming iteration does not simply inherit the optimal solution from the previous one. Consequently, an observable decay of the best solution can occur during the evolution of QGA, preventing stagnation and encouraging the search for new potential solutions.

The evolution of the QGA will terminate at a pre-defined maximum generation. However, if the evolution remains stagnant for a long time, it will be considered to have reached a local optimum and thus will be terminated. The termination criteria can vary based on the specific optimization problem. For the optimization problem discussed in this paper, we have determined that if the QGA evolution remains in a certain state for more than half of the maximum generation, the evolution will be terminated automatically.

In summary, the QGA process is described in Fig. 1.

Optimization of PML TRC

We consider the design of an N layer PML for TRC (as shown in Fig. 2a). The thickness of designed PML is 1200 nm in total. Each layer of the PML structure can be one of four candidate materials: silicon dioxide (SiO_2), silicon nitride (Si_3N_4), titanium dioxide (TiO_2), or aluminum oxide (Al_2O_3), and each material is assigned one of the combinations of two binary labels (00 = SiO_2, 01 = Si_3N_4, 10 = TiO_2, 11 = Al_2O_3). The concatenation of these binary labels in order gives a $2N$-long vector representing the structure. The optimization of PML structures is to minimize the FOM. The perfect PML can block all UV and IR light while allowing all visible light to transmit through. The proposed QGA, as an optimizer, is utilized to perform the optimization. As a comparison, we have also used CGA and QA for the same optimization problem. The details of QA can be found in Supplementary Information, Section 3.

Fig. 2(b) shows the schematic of the QGA-facilitated optimization algorithm proposed for PML optimization. The algorithm is based on active learning scheme with iterations of random forest (RF) training, QGA optimization, and TMM calculations. The details of the algorithm can be found in Method section.

We first take $N = 6$ as a benchmark study to test our algorithm, for which we can afford performing an exhaustive search by calculating the optical properties using the transfer matrix method (TMM), which is the most efficient method to calculate optical characteristics of PML structures and evaluate the FOM of every one of all the $4^6 = 4096$ possible structures.

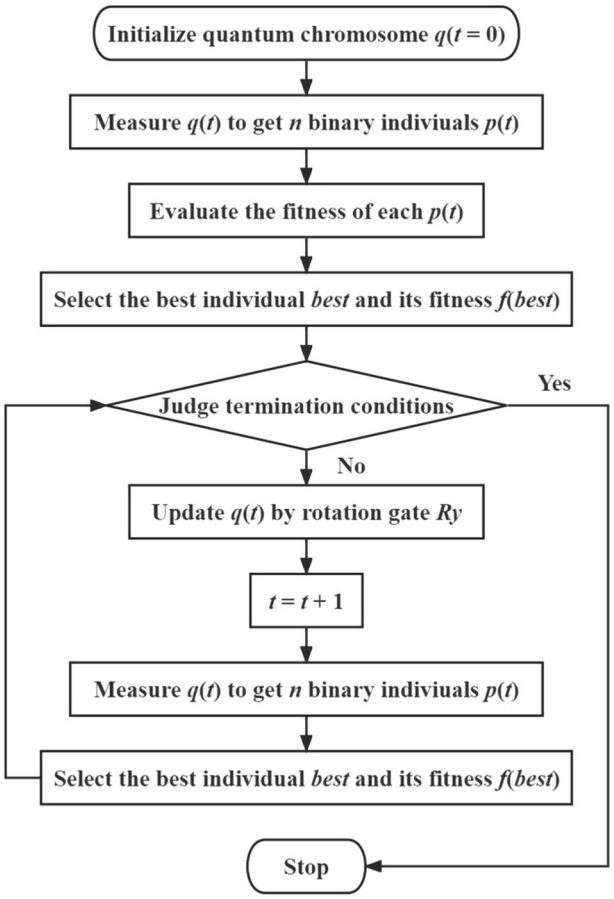

Fig. 1 | The Workflow of QGA. A quantum chromosome is first initialized, followed by the measurement and fitness evaluation of measured individuals. The best individual is selected from all the measurements, and its genetic information is used to guide the evolution of the quantum chromosome. The process repeats until the termination conditions are satisfied.

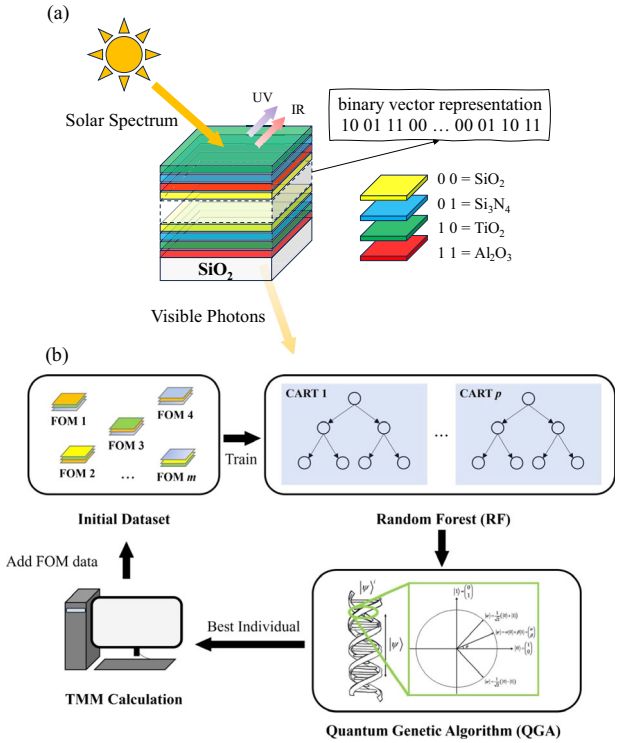

Fig. 2 | Schematics of PML TRC structure design. a The schematic structure of the PML in the TRC. With proper binary embedding for candidate materials, the PML can be mapped into a binary vector. **b** The workflow of active learning iteration between RF, QGA and TMM.

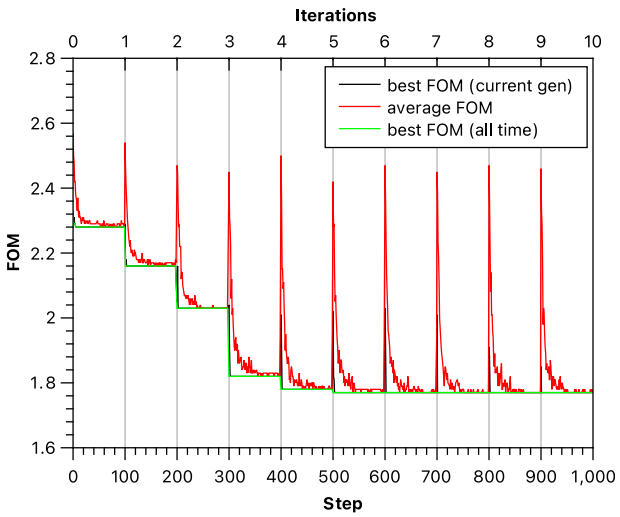

Fig. 3 | The evolution of FOM for $N = 6$ in QGA-facilitated active learning optimization. The blue curve, orange curve and green curve represent the best FOM in the current generation, the average FOM in the current generation and the best FOM of all time, respectively. In each iteration of our active learning scheme, there are 100 generations for the QGA.

The optimal structure, denoted as [10 10 00 10 01 11], is identified with a FOM of 1.7713 from this brute force exhaustive search. We then used our QGA-facilitated optimization to solve the same $N = 6$ problem. The QGA-facilitated optimization is implemented with an initial training set with the amount of data of $m = 25$ and a maximum iteration number of 10. In each generation, the quantum chromosome undergoes 25 measurements, and fitness evaluations are performed on these measurements using the RF surrogate model to discern the evolution direction of the quantum chromosome. An adaptive rotating angle, as defined in Eq. 4, decays from the upper to the lower bounds of 0.1π and 0.01π, respectively. Throughout the evolution process, the mutation rate is maintained at 0.001. The QGA terminates after 100 generations or if it reaches a converged state before that. Fig. 3 shows the evolution of FOM in the QGA optimization. The blue curve, orange curve and green curve represent the best FOM in the current generation, the average FOM in the current generation and the best FOM of all time, respectively. The x-axis is the step in the entire optimization, and each iteration of the active learning has 100 steps (correspond to 100 generations in QGA). As the figure shows, in each iteration, the FOM decays to a converged value, and the next iteration starts with a newly initialized quantum chromosome which partially include the information from the last iteration (the details of the quantum chromosomes initialization is shown by Eq. 6). After only 5 iterations, the FOM has successfully converged to 1.7713, which is consistent with the solution obtained from the exhaustive search. Compared with the 4096 TMM calculations required by the brute force exhaustive search, QGA only requires ~125 TMM calculations (details in the Methods section) in 5 active learning iterations to label the solution of each iteration before getting the global optima. This benchmark test indicates the effectiveness and efficiency of our QGA-facilitated active learning optimization scheme.

The optimization is subsequently carried out for structures with $N = 8$, 10, 16, and 20. Optimizing structures with higher N demands a larger population size and an increased number of generations in QGA. In addition, a larger initial dataset may also be needed to start the iterations efficiently. The parameters for the optimization are detailed in the

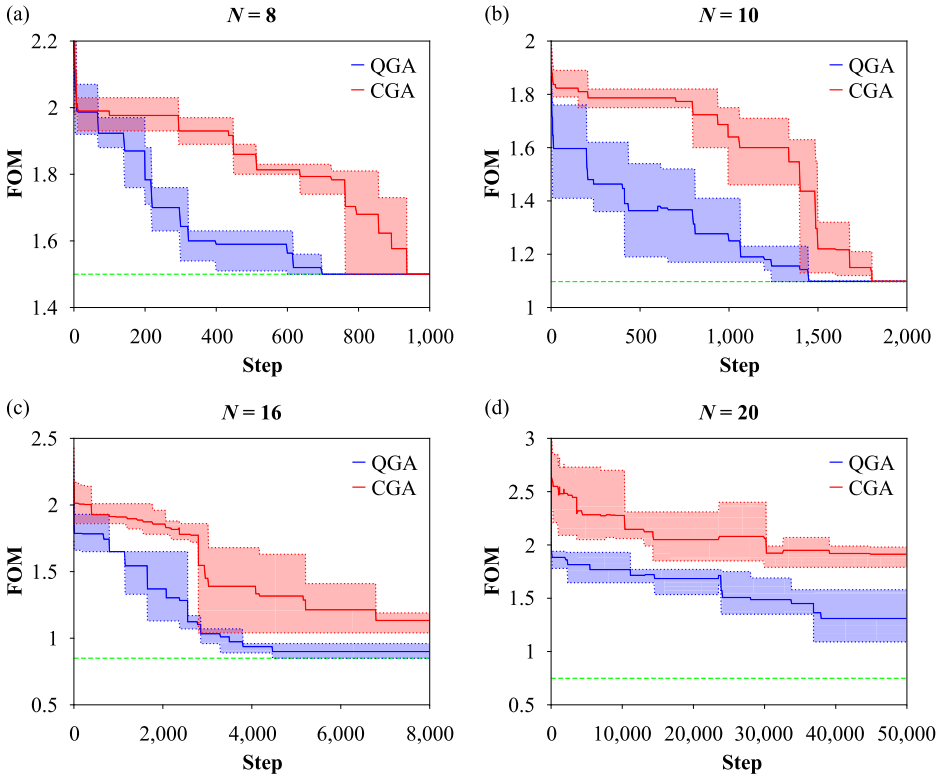

Fig. 4 | Evolution of the best FOM in QGA and CGA. Panel (**a**) ~ (**d**) represent the results of N = 8, 10, 16 and 20, respectively. The solid lines represent the average values from 5 multiple independent numerical experiments. The shadow regions represent the range of the best FOM from different trials. The horizontal green dash lines in the plots are the ground truth from exhaustive search (for N = 8 and 10) or the best solution from QA-assisted optimization algorithm (for N = 16 and 20).

Supplementary Information, section 2. Fig. 4 shows the evolution of the best FOM of all time for N = 8, 10, 16 and 20, and the long-term convergence states in the high dimensional cases are not shown to highlight the FOM evolution at the early stage. For low dimensional cases (N = 8 and 10), our algorithm can discover accurate ground state obtained from exhaustive search faster than CGA-facilitated optimizations. For higher dimensional problems (such as N = 16), our QGA algorithm can converge to the same structure as QA-facilitated optimization (using a real quantum annealer, D-Wave) within 7 iterations (under 5000 generations in total), while CGA start to fail obtaining a comparable result with QA. For the problem with N = 20, both CGA and QGA algorithms cannot find the structure that is as good as QA finds. That is because the extremely large dimension of the search space requires an extremely large number of measurements in each generation to explore, which is prohibitively computationally expensive using a classical computer. Theoretically, the randomness introduced by quantum measurements, given a sufficient number of measurements, will guide the algorithm to explore the search space. The process involved in finding a local optimum, escaping from it, and then identifying a better solution, ultimately converging to a global optimum or a proper local optimum, can be very computationally intensive and time-consuming when using a classical computer to mimic quantum operations[50]. Especially when the dimension of the problem increases, the required measurement of quantum chromosomes and the fitness evaluation of each measurement result will be the bottleneck of computational efficiency and will also be the decisive factor in whether the algorithm can converge to the optimal solution. To improve the performance of the algorithm on higher-dimensional problems, future work can focus on accelerating the measurement of quantum states, so that most of the evolution operations of QGA can be migrated to real quantum devices, greatly reducing the amount of computation undertaken by classical computers during the optimization, thereby improving the ability of QGA algorithm on high-dimensional problems. Nevertheless, due to the inherent quantum properties, QGA still outperforms CGA on both converging speed and exploring ability.

The thicknesses of all the PML TRCs discussed above are fixed at 1200 nm. However, the overall thickness of the PML structures is also important for TRC performance. We explore how varying the total thickness of the PML structure affects its performance. Specifically, 16-layer PML structures with different overall thicknesses (1200 nm, 1000 nm, and 800 nm) are optimized using the proposed algorithm. Fig. 5 shows the evolution of the best FOM in QGA for the three different PML TRCs. QA-assisted optimizations are used to benchmark optimized results for QGA-facilitated optimization. For all the three systems, out QGA-facilitated algorithm can still converge to the same solution as QA-facilitated algorithm. The effect of PML thickness on TRC performance is not monotonic. Compared to the 1200 nm structure, both the 1000 nm and 800 nm structures show better performance, with the 1000 nm structure outperforming the 800 nm structure. This makes thickness a key variable in the design of

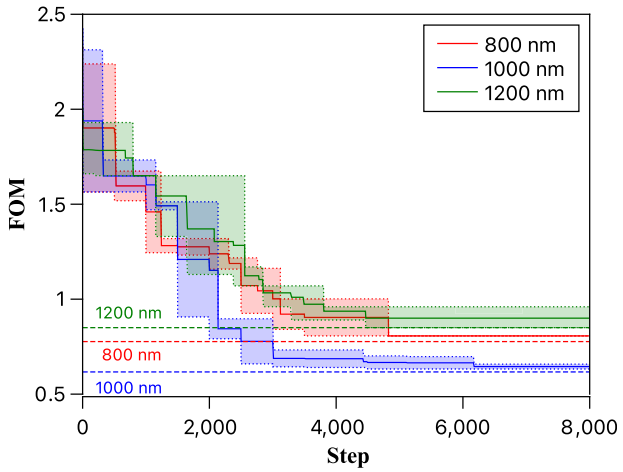

Fig. 5 | Evolution of the best FOM in QGA for 16-layer PML TRC with different thicknesses (800 nm, 1000 nm and 1200 nm). The solid lines and shadow represent the average values and the range of the best FOM from 5 multiple independent numerical experiments. Dash lines represent the results from QA-assisted optimization algorithm.

TRC materials. However, since thickness is a continuous variable, it cannot be directly optimized using QA. Therefore, developing an efficient discretization method for continuous variables such as thickness will become an important factor in applying quantum algorithms to material design. In future work, we will focus on developing discretization methods to enable the application of quantum algorithms for material design.

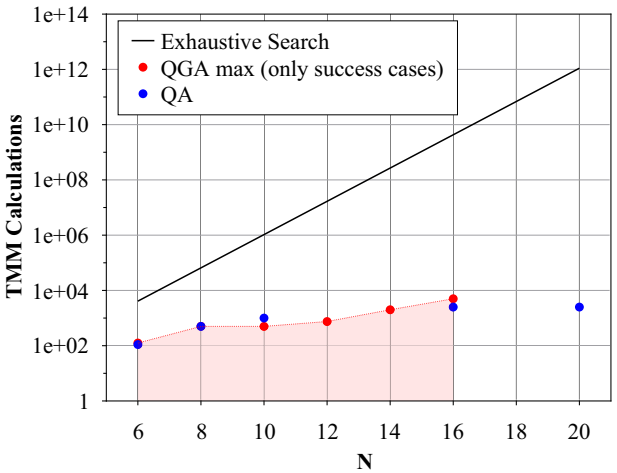

Fig. 6 | Comparison of computational cost for exhaustive search, QGA and QA. For QGA, we only take the cases that successfully converge with global optima (from exhaustive search for low dimensional cases) and QA results (for high dimensional cases). The numbers of TMM calculations in QGA-facilitated optimization are less than the max evaluation, which is the population size × iteration number.

Computational efficiency analysis

One crucial metric for evaluating the efficiency of an algorithm is its computational cost. In the context of the PML optimization using active learning, the total number of TMM calculations, which is the rate-limiting step in the iteration, serves as a key indicator of this cost. When optimizing an N-layered structure, an exhaustive search approach would necessitate 4^N TMM calculations to explore all possible solutions before identifying the true global optimum.

Fig. 6 shows the relationship between the number of required fitness evaluations by TMM calculations and the number of layers in the design by using exhaustive search, QGA and QA. For QGA, only the cases that found the global optima are counted in comparison. Note, the y-axis is plotted on a log10 scale. The efficacy of our QGA-facilitated and QA-facilitated optimization is highlighted by their substantially reduced need for TMM calculations as compared to exhaustive search methods. This advantage is further amplified by the high-performance nature of the RF model, which enables the max required TMM calculation by the QGA-facilitated optimization algorithm basically the same order of magnitude as the QA-assisted optimization algorithm, but during the optimizations, the QGA-facilitated algorithm requires even fewer TMM calculations as the it gradually converges to the optimal structure and producing repeated solutions in the labeling. This results in a significant alleviation of the burden traditionally associated with data acquisition, which is the TMM calculation in our case, but can be other physics-based modeling or experiments in other optimization tasks. This advantage is believed to be from the accuracy of the surrogate model, which is further discussed in the next section.

Comparison between random forest (RF) and factorization machine (FM) model

Although the QGA's global search capability is currently not as good as QA in the high dimension optimization cases, the superiority of the RF model over factorization machine (FM), which is the required surrogate for QA as

Fig. 7 | Comparison between FM and RF models prediction RMSE. Panel (**a**) ~ (**d**) show the comparisons for (**a**) $N = 8$, (**b**) $N = 10$, (**c**) $N = 16$, and (**d**) $N = 20$. RMSE is evaluated on the same test dataset for FM and RF models. The error bars are calculated from the results of 10 independent experiments.

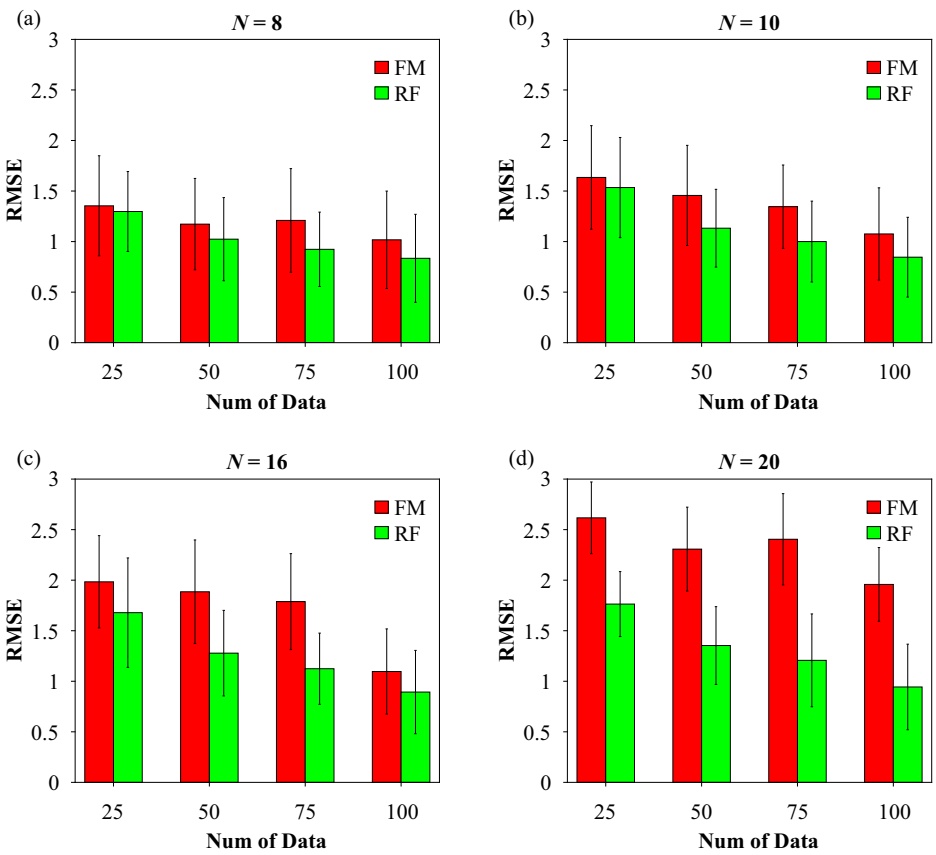

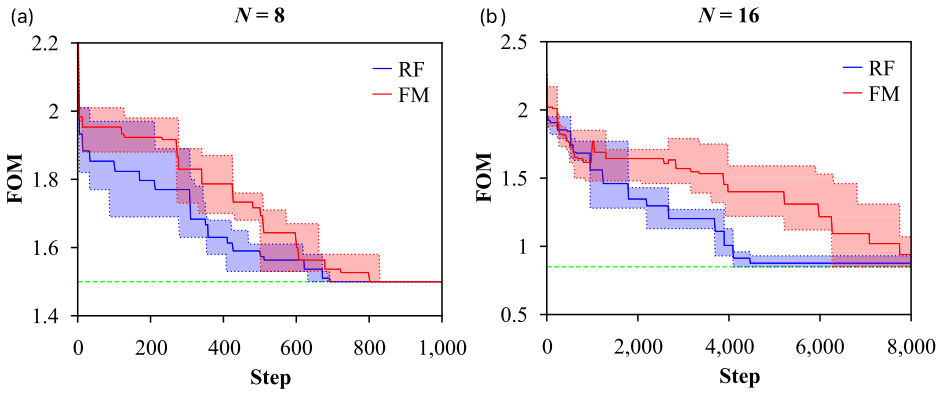

Fig. 8 | QGA evolution with RF surrogate model and FM surrogate model. a $N = 8$ and (**b**) $N = 16$. Solid lines and shadows represent average FOM evolution and range of multiple trials.

it can be mapped into a QUBO formulation, affords our proposed QGA-facilitated optimization algorithm a more reliable searching landscape for high-dimensional problems. Fig. 7 provides a comparative analysis of the Rooted Mean Squared Error (RMSE) for FM and RF. Both are trained using TMM-calculated FOM data from of 8-layer, 10-layer, 16-layer, and 20-layer structures, with varying numbers of data points (25, 50, 75, and 100) randomly selected. 10 independent experiments have been performed and the standard errors of the mean are calculated as the error bars. Training is implemented with 5-fold cross-validation and Stochastic Gradient Descent (SGD), and RMSE is evaluated on a randomly selected test set. The results show that RF models outperform FM on the test sets. Moreover, as the data dimensionality increases, the advantages of RF become more apparent. From Fig. 7, especially in panels (c) and (d), it can be seen that the RF model trained with less data can achieve higher accuracy than the FM model trained with more data, which indicates that the RF model requires less data to achieve higher prediction accuracy than FM model, which should be the reason why fewer iterations are necessary in our QGA-facilitated optimization algorithm than the QA-assisted optimization.

To further confirm this hypothesis, the trained RF and FM models are subsequently employed as surrogate models for the QGA in optimizing PML structures with dimensions of $N = 8$ and 16. Fig. 8 illustrates the evolution curves of QGA when utilizing RF and FM as surrogate models with the same initialization. It can be observed that for the low-dimensional problem of $N = 8$, QGA always converges to the optimal structure regardless of the surrogate model employed, and the converging speed using RF is faster than FM. However, for the higher-dimensional scenario ($N = 16$), employing RF as the surrogate model enhances the speed of QGA's convergence greatly. This substantiates the advantage of using RF as a more general surrogate model over FM.

Energy Saving Analysis

Lastly, we estimated the benefit of the 16-layer and 20-layer TRC designed by our algorithm as a potential window material by calculating the energy it can save annually in the U.S. using EnergyPlus[24,51]. The annual energy saving over the surveyed U.S. cities is shown in Fig. 9a, b. On average, the application of the 16-layer TRC as a window material would yield an annual energy saving of 33.58 MJ/m^2 over the surveyed locations. Even for the 20-layer TRC structure, despite not reaching the global minimum, can still contribute to an average annual energy saving of 26.03 MJ/m^2. Fig. 9c, d show the energy savings for the top 15 energy consuming states in the U.S. For the hot states (e.g., Arizona, Nevada, and Hawaii), our designed 16-layer TRC can potentially save ~30% of the cooling energy compared to conventional windows. The same calculations have also been performed for 20-layer TRC, and an energy saving over 20% can be achieved. Fig. 9e shows the comparison between the transmitted irradiance through the ideal and our optimized 16-layer and 20-layer TRCs. The transmitted irradiance of the 16-layer structure has better alignment with the ideal TRC, showing better performance than the 20-layer structure.

Towards More Applications – Optimization of Optical Diodes

In addition to the application in the TRC design, our QGA-facilitated optimization algorithm can be applied to other material design problems. Here, we test the performance of our algorithm on designing metamaterials optical diodes. Nanophotonic structures that exhibit asymmetrical power (intensity) transmission can be considered optical diodes, following the concept of electrical or thermal diodes that have asymmetrical transport properties[52–54]. An optical diode permits the intensity of light to transmit in one direction (i.e., forward direction) but blocks it in the reverse direction (i.e., backward direction). The FOM of an optical diode can be defined as the difference between the forward (T_F) and backward (T_B) transmissivities (i.e., FOM = T_F - T_B)[55], and a larger FOM indicates the better performance of the optical diode.

The stratified volume diffractive film composed of metal and dielectric materials can be considered as a system for optical diodes. Fig. 10a shows the schematic structure of the thin-film optical diode with a stratified volume diffractive film, in which it has a unit cell consisting of metallic gratings and a dielectric spacer. Fig. 10b shows the configuration of the unit cell, which is discretized with rectangular pixels, as proposed by Kim et al. in ref. [55]. The material selection of a pixel can be encoded into a binary digit as "0" for a dielectric or "1" for a metal medium. The pixelated metamaterial structure is then represented by a binary vector with a length of N. FOMs of the structures are calculated using the rigorous coupled-wave analysis (RCWA) method[56]. Here, we test our algorithm on two cases: wavelength $\lambda = 600$ nm ($N = 40$) and 800 nm ($N = 32$). Fig. 10c shows the evolution of the best FOM as a function of optimization steps for both cases. For these high dimensional optimization problems, although still limited by computational resources to find the same optimal structures as QA-assisted optimization algorithm found (0.8064 for $\lambda = 600$ nm, 0.8648 for $\lambda = 800$ nm), our algorithm can still lead the exploration of the design space towards the right direction within 50 iterations (the population sizes are 200 in both cases). The number of RCWA calculations in the QGA-facilitated algorithm is under 10,000 in both cases, which are in the same order of magnitude as the thousands of RCWA calculations needed for the QA-assisted algorithm. Comparing with CGA-facilitated optimization, our QGA-facilitated algorithm can still converge faster to better optimal structures, which has been already been shown in the TRC case.

Discussion

In this work, we introduce an optimization algorithm based on QGA to address the challenge of finding the optimal in binary combinatorial problems. We used PML for TRC as an application example. The combination of QGA and RF regression model iteratively operates in an active learning framework to obtain global optimum in complex and discrete search spaces. QGA excels in aspects like smaller population size, faster convergence speed, superior global search ability, and robustness, greatly outperforming conventional genetic algorithms. Moreover, compared to employing FM (QUBO) to describe the search space, the RF regression model demonstrates

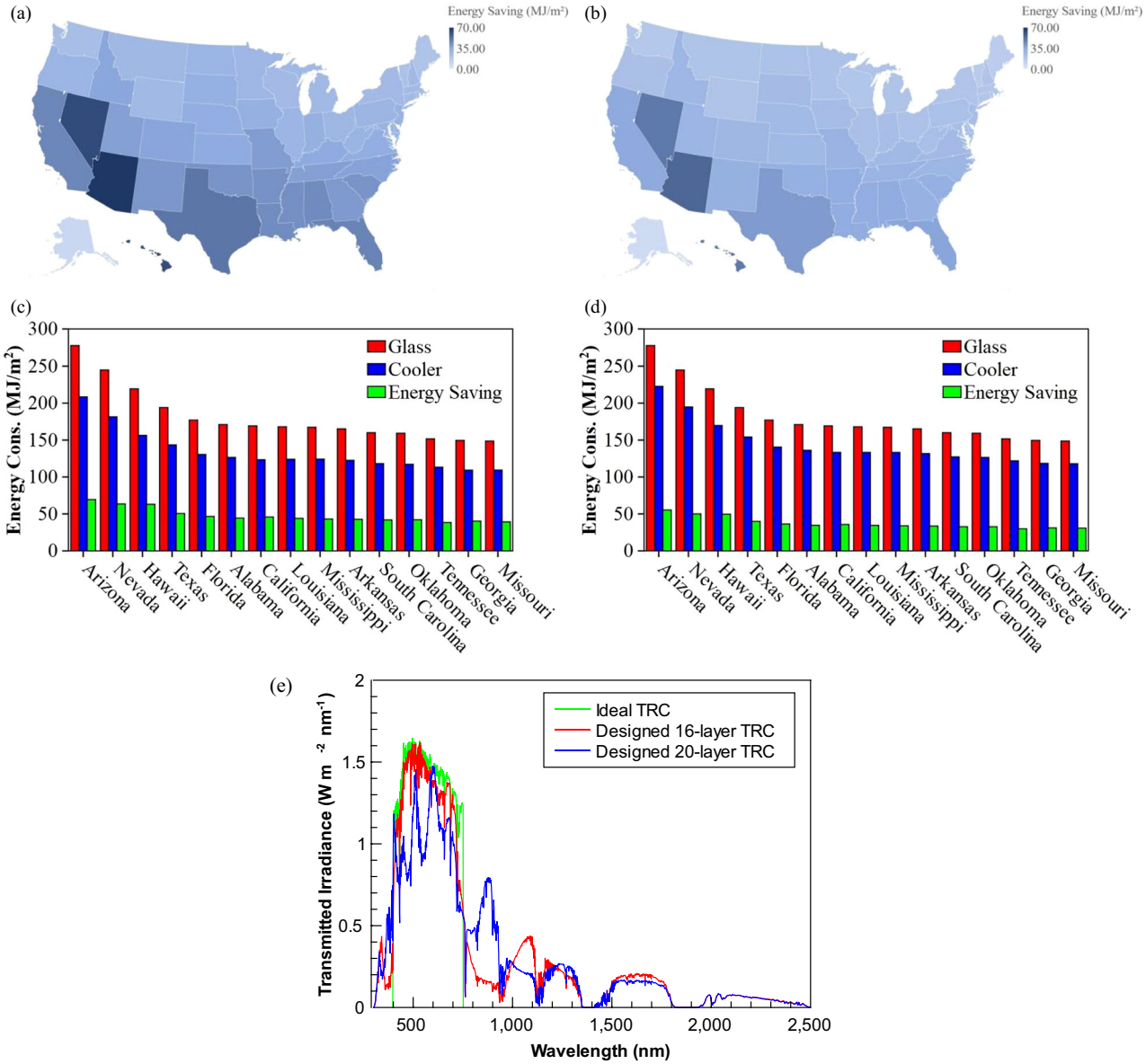

Fig. 9 | Energy saving analysis for design PML TRC structures. Panel (**a**) and (**b**) show the estimated cooling energy saving across the U.S. by using the 16-layer and 20-layer TRC as the window material, respectively. The annual energy savings of the top 15 energy-consuming states over U.S. by applying (**c**) the 16-layer TRC and (**d**) the 20-layer TRC designed by our QGA-facilitated optimization. **e** The transmitted irradiance through the target ideal and our optimized 16-layer and 20-layer TRCs by QGA-facilitated active learning scheme.

stronger reliability in high-dimensional problems. Hence, unless the dimensionality of the problem is unreachable for classical computers, QGA can be more efficient compared QA not to mention CGA. Furthermore, any predictive model that is well-suited for accepting binary vectors as input will be accessible for our QGA-based optimization framework, and this will provide more freedom when compared with QA-based optimization. At the same time, the results in this work point out the bottleneck of current QA-facilitated optimization scheme and strongly indicate the necessity for developing FM that with 3rd or higher orders and accessible by quantum annealers.

Methods

Quantum computing

Quantum computing, an intriguing application of quantum mechanics in algorithmic computation, significantly diverges from classical computing primarily due to its intrinsic parallelism. Unlike classical computing where systems exist in definite states, quantum computing operates on the principles of superposition and entanglement, allowing the system to exist in multiple states simultaneously[57–59]. The state of a quantum system is described by a probabilistic wave function, the square of which provides the probabilities for the possible states[28]. This attribute expedites computation in quantum systems by order of magnitude compared to classical systems.

The evolution of qubits through so-called quantum channels is carried out by unitary quantum gates that manipulate the qubits just like classical bits are manipulated by logic gates in a computer[60,61]. These unique characteristics of quantum computing – superposition, entanglement, and quantum gate operations – confer it with unparalleled computational power[62]. Integrating quantum principles into optimization algorithms offers potential improvements, enhancing traditional methods and aiding in complex problem-solving.

The basic unit for information storage is qubit in the quantum computer. Unlike classical bits that can be in a state of either 0 or 1, a qubit can exist in a state of superposition, representing 0 and 1 simultaneously. The

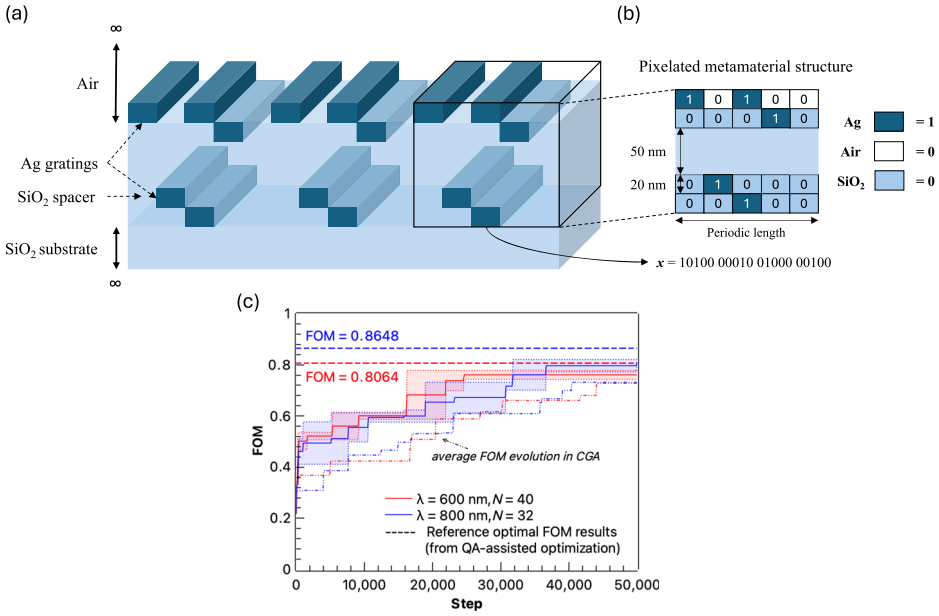

Fig. 10 | Schematics of optical diode design. a the thin-film optical diode with a stratified volume diffractive film for optimization and (**b**) the pixelated unit cell of the structure. **c** Evolution of FOM in QGA-facilitated algorithm for 600 nm and 800 nm wavelength. The dimensions of the binary vector are $N = 40$ and $N = 32$, respectively. The average FOM evolutions of the two cases in CGA-facilitated optimizations are compared with that in QGA-facilitated optimizations.

super position state of a qubit can be expressed as follows:

$$|\varphi\rangle = a|0\rangle + b|1\rangle \tag{9}$$

where, $|\varphi\rangle$ is the superposition state. a and b are complex numbers which denote the probability amplitudes of the corresponding ground state $|0\rangle$ or $|1\rangle$, and $|a|^2 + |b|^2 = 1$. Therefore, an n-qubits quantum register can store the quantum state which is the coherent superposition of 2^n ground states:

$$|\phi\rangle = \sum_{i=1}^{2^n} c_i|\phi_i\rangle \tag{10}$$

where c_i are the probability amplitudes that satisfying:

$$\sum_{i=1}^{2^n} |c_i|^2 = 1 \tag{11}$$

If we use a binary vector to encode qubits on the polymorphic problem, the system with n qubits can be expressed as follows[63]:

$$q = \begin{bmatrix} a_1 & a_2 & a_3 & \cdots & a_n \\ b_1 & b_2 & b_3 & & b_n \end{bmatrix} \tag{12}$$

where $|a_k|^2 + |b_k|^2 = 1$ ($k = 1, 2, \ldots, n$), and each pair of probability amplitudes $[a_k, b_k]^T$ represent a qubit in the system. When the quantum system is measured, coherence will disappear, and the quantum system will collapse to a definite state $|\Phi_i\rangle$ with probability given by the squared magnitude of the respective probability amplitude $|c_i|^2$ according to Eq. 10. The probability of qubit k being measured in state $|0\rangle$ (or $|1\rangle$) will be $|a_k|^2$ (or $|b_k|^2$) as Eq. 12 described.

Random forest algorithm

Decision trees, particularly the Classification and Regression Tree (CART) method, are known for their simplicity and interpretability in supervised learning[64,65]. To counter the potential overfitting problem of single decision tree, the Random Forest (RF) algorithm, which was proposed by Breiman et al. [66] in 2001, is always employed as an ensemble method to enhance model robustness and predictive accuracy. The RF algorithm operates by constructing a multitude of decision trees and averaging related predictions from individual trees, and therefore it will yield a more accurate final prediction than any individual tree could offer[67–69].

Active learning scheme with RF and QGA

We employ an optimization algorithm based on the active learning framework. To circumvent the computationally intensive TMM calculation, we implement a RF as a surrogate model, significantly accelerating the calculation speed[12,70] of the FOM per instance. Initially, the RF model is trained on m data points calculated by the TMM. Due to the limited quantity of training data, the accuracy of the Random Forest is not expected to be high initially or whole optimization space. Therefore, an iterative process between QGA and RF training is implemented within the active learning loop. During each iteration, the FOM of individuals in the QGA is evaluated using RF. The FOM calculated by RF surrogate model is mapped to the fitness value in the QGA, and all the optimal structures found in each QGA generation having lower FOMs than the best structure have found before will be recorded and the latest n solutions will be put into the TMM calculations to label true FOM, which added to the database to train a new RF model, thereby promoting the progression of iterations. The number of labeled optimal structures after each QGA evolution, n, is set to be the same as population size. Therefore, the max number of TMM calculations in the QGA-facilitated algorithm is total iteration numbers to get converged × the population size in each QGA generation.

In the algorithm, the structures of the TRC are represented by a series of binary vectors, which are also the input of TMM and RF calculations. After training the RF model, the QGA starts with the quantum chromosome initialized according to Eq. 6, and the fitness evaluation in the QGA evolution is implemented by the surrogated RF model. After obtaining the best solution from QGA, TMM is called to verify the FOM of the best solution and add the data to the training set to retrain the RF model. If the solution of QGA has been included in the training set, a randomly selected structure and its FOM is added to the training set to further diversify the applicability of the RF model in the optimization space. With the iterations ongoing, the accuracy of RF will be improved in the design space, by which the fitness evaluation will be more reliable for finding the best solution.

Data availability

Requests for data and materials should be sent to the corresponding authors or Z.X. (zxu8@nd.edu).

Code availability

The underlying codes for this study are available from the corresponding author or Z.X. (zxu8@nd.edu) upon reasonable request.

Received: 21 February 2024; Accepted: 24 October 2024;
Published online: 13 November 2024

References

1. Pope, M. A. & Aksay, I. A. Structural design of cathodes for Li-S batteries. *Adv. Energy Mater.* **5**, 1500124 (2015).
2. Zhang, X. et al. Multiscale understanding and architecture design of high energy/power lithium-ion battery electrodes. *Adv. Energy Mater.* **11**, 2000808 (2021).
3. Fayaz, H. et al. Optimization of thermal and structural design in lithium-ion batteries to obtain energy efficient battery thermal management system (BTMS): a critical review. *Arch. Comput. Methods Eng.* **29**, 129–194 (2022).
4. Liu, D., Tan, Y., Khoram, E. & Yu, Z. Training Deep Neural Networks for the Inverse Design of Nanophotonic Structures. *ACS Photonics* **5**, 1365–1369 (2018).
5. Liu, Z., Zhu, D., Rodrigues, S. P., Lee, K.-T. & Cai, W. Generative Model for the Inverse Design of Metasurfaces. *Nano Lett.* **18**, 6570–6576 (2018).
6. Ma, W., Cheng, F. & Liu, Y. Deep-Learning-Enabled On-Demand Design of Chiral Metamaterials. *ACS Nano* **12**, 6326–6334 (2018).
7. Kudyshev, Z. A., Kildishev, A. V., Shalaev, V. M. & Boltasseva, A. Machine learning–assisted global optimization of photonic devices. *Nanophotonics* **10**, 371–383 (2021).
8. So, S. & Rho, J. Designing nanophotonic structures using conditional deep convolutional generative adversarial networks. *Nanophotonics* **8**, 1255–1261 (2019).
9. Liu, Z., Zhu, Z. & Cai, W. Topological encoding method for data-driven photonics inverse design. *Opt. Express* **28**, 4825–4835 (2020).
10. Ma, W., Cheng, F., Xu, Y. & Wen, Q. & Liu, Y. Probabilistic Representation and Inverse Design of Metamaterials Based on a Deep Generative Model with Semi-Supervised Learning Strategy. *Adv. Mater.* **31**, 1901111 (2019).
11. Ma, W. & Liu, Y. A data-efficient self-supervised deep learning model for design and characterization of nanophotonic structures. *Sci. China Phys., Mech. Astron.* **63**, 284212 (2020).
12. Wiecha, P. R., Arbouet, A., Girard, C. & Muskens, O. L. Deep learning in nano-photonics: inverse design and beyond. *Photon. Res.* **9**, B182–B200 (2021).
13. Deng, L., Xu, Y. & Liu, Y. Hybrid inverse design of photonic structures by combining optimization methods with neural networks. *Photonics Nanostruct. - Fundamentals Appl.* **52**, 101073 (2022).
14. Ma, W. et al. Deep learning for the design of photonic structures. *Nat. Photonics* **15**, 77–90 (2021).
15. Mahrous, H. et al. A Multi-Objective Genetic Algorithm Approach for Silicon Photonics Design. *Photonics* **11**, 80 (2024).
16. Ren, Y. et al. Genetic-algorithm-based deep neural networks for highly efficient photonic device design. *Photon. Res.* **9**, B247–B252 (2021).
17. Cai, H., Sun, Y., Wang, X. & Zhan, S. Design of an ultra-broadband near-perfect bilayer grating metamaterial absorber based on genetic algorithm. *Opt. Express* **28**, 15347–15359 (2020).
18. Sonmez, F. O. & Tan, C. Structural optimization using simulated annealing. *Simulated annealing* **2008**, 281–306 (2008).
19. Sonmez, F. O. Shape optimization of 2D structures using simulated annealing. *Computer methods Appl. Mech. Eng.* **196**, 3279–3299 (2007).
20. Katoch, S., Chauhan, S. S. & Kumar, V. A review on genetic algorithm: past, present, and future. *Multimed. tools Appl.* **80**, 8091–8126 (2021).
21. Kadowaki, T. & Nishimori, H. Quantum annealing in the transverse Ising model. *Phys. Rev. E* **58**, 5355–5363 (1998).
22. Tanaka, S., Tamura, R. & Chakrabarti, B. K. *Quantum spin glasses, annealing and computation*. (Cambridge University Press, 2017).
23. Albash, T. & Lidar, D. A. Adiabatic quantum computation. *Rev. Mod. Phys.* **90**, 015002 (2018).
24. Kim, S. et al. High-Performance Transparent Radiative Cooler Designed by Quantum Computing. *ACS Energy Lett.* **7**, 4134–4141 (2022).
25. Narayanan, A. & Moore, M. in *Proceedings of IEEE International Conference on Evolutionary Computation*. 61-66.
26. Han, K.-H. & Kim, J.-H. Genetic Quantum Algorithm and its Application to Combinatorial Optimization Problem. 1354–1360 (2003).
27. Lv, Y. & Li, D. in *2008 Fourth International Conference on Natural Computation*. 460–464 (IEEE).
28. Wang, H., Liu, J., Zhi, J. & Fu, C. The Improvement of Quantum Genetic Algorithm and Its Application on Function Optimization. *Math. Probl. Eng.* **2013**, 730749 (2013).
29. Raman, A. P., Anoma, M. A., Zhu, L., Rephaeli, E. & Fan, S. Passive radiative cooling below ambient air temperature under direct sunlight. *Nature* **515**, 540–544 (2014).
30. Li, W., Li, Y. & Shah, K. W. A materials perspective on radiative cooling structures for buildings. *Sol. Energy* **207**, 247–269 (2020).
31. Lee, M. et al. Photonic structures in radiative cooling. *Light.: Sci. Appl.* **12**, 134 (2023).
32. Vall, S., Medrano, M., Solé, C. & Castell, A. Combined Radiative Cooling and Solar Thermal Collection: Experimental Proof of Concept. *Energies* **13**, 893 (2020).
33. Arrés Chillón, J., Paulillo, B., Mazumder, P. & Pruneri, V. Transparent Glass Surfaces with Silica Nanopillars for Radiative Cooling. *ACS Appl. Nano Mater.* **5**, 17606–17612 (2022).
34. Lei, M.-Q. et al. Transparent radiative cooling films containing poly(methylmethacrylate), silica, and silver. *Optical Mater.* **122**, 111651 (2021).
35. Jaramillo-Fernandez, J. et al. Highly-Scattering Cellulose-Based Films for Radiative Cooling. *Adv. Sci.* **9**, 2104758 (2022).
36. Jin, Y., Jeong, Y. & Yu, K. Infrared-reflective transparent hyperbolic metamaterials for use in radiative cooling windows. *Adv. Func. Mater.* **33**, 2207940 (2022).
37. Chen, Z., Zhu, L., Raman, A. & Fan, S. Radiative cooling to deep sub-freezing temperatures through a 24-h day–night cycle. *Nat. Commun.* **7**, 13729 (2016).
38. Zhai, Y. et al. Scalable-manufactured randomized glass-polymer hybrid metamaterial for daytime radiative cooling. *Science* **355**, 1062–1066 (2017).
39. Li, T. et al. A radiative cooling structural material. *Science* **364**, 760–763 (2019).
40. Tikhonravov, A. V., Trubetskov, M. K. & DeBell, G. W. Application of the needle optimization technique to the design of optical coatings. *Appl. Opt.* **35**, 5493–5508 (1996).
41. Tikhonravov, A. V. Some theoretical aspects of thin-film optics and their applications. *Appl. Opt.* **32**, 5417–5426 (1993).
42. Li, W., Shi, Y., Chen, Z. & Fan, S. Photonic thermal management of coloured objects. *Nat. Commun.* **9**, 4240 (2018).
43. Shi, Y., Li, W., Raman, A. & Fan, S. Optimization of Multilayer Optical Films with a Memetic Algorithm and Mixed Integer Programming. *ACS Photonics* **5**, 684–691 (2018).
44. Wang, H., Zheng, Z., Ji, C. & Jay Guo, L. Automated multi-layer optical design via deep reinforcement learning. *Mach. Learn.: Sci. Technol.* **2**, 025013 (2021).
45. Kitai, K. et al. Designing metamaterials with quantum annealing and factorization machines. *Phys. Rev. Res.* **2**, 013319 (2020).
46. Zhang, G. Quantum-inspired evolutionary algorithms: a survey and empirical study. *J. Heuristics* **17**, 303–351 (2011).
47. Choe, I.-H. et al. Can quantum genetic algorithm really improve quantum backpropagation neural network? *Quantum Inf. Process.* **22**, 154 (2023).
48. Xu, Z. & Zhou, X. Determination of the Critical Slip Surface of Slope Based on the Improved Quantum Genetic Algorithm and Random Forest. *KSCE J. Civ. Eng.* **26**, 2126–2138 (2022).
49. Shu, W. & He, B. 169–176 (Springer).

50. Saad, H. M. H., Chakrabortty, R. K., Elsayed, S. & Ryan, M. J. Quantum-Inspired Genetic Algorithm for Resource-Constrained Project-Scheduling. *IEEE Access* **9**, 38488–38502 (2021).
51. Kim, S., Jung, S., Bobbitt, A., Lee, E. & Luo, T. Wide-angle spectral filter for energy-saving windows designed by quantum annealing-enhanced active learning. *Cell Rep. Phys. Sci.* **5**, 101847 (2024).
52. Jalas, D. et al. What is—and what is not—an optical isolator. *Nat. Photonics* **7**, 579–582 (2013).
53. Zhang, T. & Luo, T. Giant thermal rectification from polyethylene nanofiber thermal diodes. *Small* **11**, 4657–4665 (2015).
54. Shrestha, R. et al. Dual-mode solid-state thermal rectification. *Nat. Commun.* **11**, 4346 (2020).
55. Kim, S. et al. Quantum annealing-aided design of an ultrathin-metamaterial optical diode. *Nano Convergence* **11**, 16 (2024).
56. Moharam, M., Gaylord, T., Grann, E. B. & Pommet, D. A. Formulation for stable and efficient implementation of the rigorous coupled-wave analysis of binary gratings. *J. Optical Soc. Am. A* **12**, 1068–1076 (1995).
57. Preskill, J. Quantum computing in the NISQ era and beyond. *Quantum* **2**, 79 (2018).
58. Shor, P. W. Quantum computing. *Doc. Mathematica* **1**, 1 (1998).
59. Yang, S. Y., Liu, F. & Jiao, L. C. Novel genetic algorithm based on the quantum chromosome. *J. Xidian Univ.* **31**, 76–81 (2004).
60. Nielsen, M. A. & Chuang, I. L. *Quantum computation and quantum information*. (Cambridge University Press, 2010).
61. DiVincenzo, D. P. The Physical Implementation of Quantum Computation. *Fortschr. der Phys.* **48**, 771–783 (2000).
62. Schuld, M., Sinayskiy, I. & Petruccione, F. The quest for a Quantum Neural Network. *Quantum Inf. Process.* **13**, 2567–2586 (2014).
63. Zhang, G. & Rong, H. in *Computational Science – ICCS 2007*. (eds Y. Shi, G. D. van Albada, J. Dongarra, & P. M. A. Sloot) 243-250 (Springer Berlin Heidelberg).
64. Lewis, R. J. (Citeseer).
65. Steinberg, D. & Colla, P. CART: classification and regression trees. *top. ten algorithms data Min.* **9**, 179 (2009).
66. Breiman, L. Random Forests. *Mach. Learn.* **45**, 5–32 (2001).
67. Lagomarsino, D., Tofani, V., Segoni, S., Catani, F. & Casagli, N. A Tool for Classification and Regression Using Random Forest Methodology: Applications to Landslide Susceptibility Mapping and Soil Thickness Modeling. *Environ. Modeling Assess.* **22**, 201–214 (2017).
68. Matin, S. S., Farahzadi, L., Makaremi, S., Chelgani, S. C. & Sattari, G. Variable selection and prediction of uniaxial compressive strength and modulus of elasticity by random forest. *Appl. Soft Comput.* **70**, 980–987 (2018).
69. Mercadier, M. & Lardy, J.-P. Credit spread approximation and improvement using random forest regression. *Eur. J. Operational Res.* **277**, 351–365 (2019).
70. Peng, C., Li, Y., Cao, L. & Jiao, L. in *2019 IEEE congress on evolutionary computation (CEC)*. 1060–1067 (IEEE).

Acknowledgements

This research was supported by the Quantum Computing Based on Quantum Advantage Challenge Research (RS-2023-00255442) through the National Research Foundation of Korea (NRF) funded by the Korean government (Ministry of Science and ICT(MSIT)). This research also used resources of the Oak Ridge Leadership Computing Facility at the Oak Ridge National Laboratory, which is supported by the Office of Science of the U.S. Department of Energy under Contract No. DE-AC05-00OR22725. The authors also would like to thank the Notre Dame Center for Research Computing for supporting all the simulations in this work. Notice: This manuscript has in part been authored by UT-Battelle, LLC under Contract No. DE-AC05-00OR22725 with the U.S. Department of Energy. The United States Government retains and the publisher, by accepting the article for publication, acknowledges that the U.S. Government retains a non-exclusive, paid up, irrevocable, world-wide license to publish or reproduce the published form of the manuscript, or allow others to do so, for U.S. Government 15 purposes. The Department of Energy will provide public access to these results of federally sponsored research in accordance with the DOE Public Access Plan (http://energy.gov/downloads/doe-publicaccess-plan).

Author contributions

Z.X., E.L., and T.L. conceived the idea; Z.X. designed and performed the QGA code for the research; W.S. and S.K. performed the QA for the research; A.B. performed the energy saving calculations; Z.X. wrote most parts of the manuscript; All authors discussed the results and commented on the manuscript.

Competing interests

The authors declare no competing interests.

Additional information

Supplementary information The online version contains supplementary material available at https://doi.org/10.1038/s41524-024-01438-9.

Correspondence and requests for materials should be addressed to Eungkyu Lee or Tengfei Luo.